Metal-Coated Fiber-Optic Platforms for Surface Plasmon Polariton Generation and Interconnection

Hyuntai Kim and Yoonchan Jeong, *Member, IEEE*

***Abstract*— We analyze a novel metal-coated fiber-optic platform for surface plasmon polariton (SPP) generation and interconnection. It is based on a metal-coated angled fiber facet (MCAFF), which enables alignment-free and unidirectional SPP generation from a fiber-optic mode with high conversion efficiency. We verify its functionality by means of both numerical simulation and preliminary experiment. We implement a two-level-thickness (TLT) configuration into the MCAFF to maintain its high optic-to-plasmonic conversion efficiency: The thin metallic layer just above the core region efficiently generates SPPs whilst the thick metallic layer beyond the core region enables its low-loss propagation by diminishing decoupling possibility into the dielectric region. We moreover devise a fiber-in-fiber-out (FIFO) platform that consists of a pair of TLT-MCAFFs. We numerically verify that it can yield more than 60% of FIFO coupling efficiency. We further show that the transmission spectrum of the FIFO-MCAFF is highly correlated with the refractive index of the top layer put on the metallic layer, and that it can be exploited to sensing applications that is required to measure and identify delicate changes in the refractive index of the top-layer material. We expect that the proposed metal-coated fiber-optic platforms will provide an efficient way to SPP generation and interconnection, and also has great potential to be novel sensing platforms for gas- or liquid-phase volatile substance.**

***Index Terms*— Surface plasmon polariton generation, optical fiber, nanophotonics, plasmonic sensing.**

I. Introduction

SURFACE plasmon polaritons (SPPs), a group of collectively oscillating electrons at a dielectric-metal interface, have been extensively studied thanks to their extraordinary physical characteristics and their high-end applications [1]–[8]. As their wavenumbers are invariably larger than their free-space counterparts, SPPs are normally generated by means of very special coupling techniques [1], [2]. Some of the common SPP-coupling schemes include prism-coupling, nano-aperture, and grating-assisted schemes [9]–[11]. However, these conventional SPP-coupling schemes inevitably have considerable limitations in terms of compactness, flexibility, efficiency, controllability, etc. [1]–[3]. Thus, to resolve such drawbacks, alternative SPP-coupling schemes exploiting optical fiber platforms have extensively been studied in recent years, which can naturally make use of the advantages of optical fibers such as flexibility, reliability, compatibility, ease of alignment, etc. [12]–[23]. Most of the studies utilized a nano-aperture structure built upon a metal-coated fiber facet [12]–[15] although its SPP-coupling efficiency tended to be low owing to generation of non-confined diffraction light, bi-directional coupling of SPPs, and reflection loss by the small aperture size [15]. More recently, we have proposed a metal-coated angled fiber facet (MCAFF) coupling technique [16]–[20], showing that the MCAFF technique can significantly resolve out the low-efficiency issue with the nano-aperture schemes. However, our preceding studies were limited to the analysis of the basic functionality of an MCAFF via simplified justification and demonstration.

Here, in this paper, building upon our previous proposition and studies, we aim to detail out the characteristics of an MCAFF in more generalized conditions. Moreover, extending our numerical model to a dual-fiber platform, we rigorously characterize a novel fiber-in-fiber-out (FIFO) platform for plasmonic interconnection and sensing.

II. Generation of Surface Plasmon Polaritons

In general, Kretschmann's configuration can generate unidirectional SPPs with good efficiency [1], [9]. However, it relies primarily on free-space optics, so that it requires elaborate instrumentation and preparation in order to obtain SPPs on a specific position targeted. Moreover, the size of the resultant SPP spot tends to be relatively large as it normally uses a collimated Gaussian beam or a plane wave. To overcome these drawbacks, we proposed to replace the bulk-type prism with an angled fiber in our previous reports [16]–[20]. This scheme can readily offer an alignment-free platform for generating SPPs once the fiber facet angle is appropriately determined. Furthermore, utilizing optical fibers of different core dimensions, one can control the SPP spot size as small as desired. We stress that this MCAFF scheme can significantly enhance the conversion efficiency between optical fiber modes and SPPs in comparison with the conventional nano-aperture fiber schemes [15], [20]. In fact, the operation principle of the MCAFF scheme is quite similar to that of Kretschmann's configuration [1], [9], such

Manuscript received October 7, 2019; revised December 15, 2019; accepted January 12, 2020. Date of publication January 23, 2020; date of current version February 10, 2020. This work was supported in part by the National Research Foundation (NRF) funded by the Korean Ministry of Science, ICT under Grant 2017R1D1A1B03036201 and Grant 2019R1F1A1063151, in part by the BK21 Plus, and in part by the 2020 Hongik University Research Fund. *(Corresponding author: Yoonchan Jeong.)*

Hyuntai Kim is with the Department of Electronic and Electrical Convergence Engineering, Hongik University, Sejong 30016, South Korea.

Yoonchan Jeong is with the Department of Electrical and Computer Engineering, Seoul National University, Seoul 06288, South Korea, and also with the IAP/ISRC/GSEP, Seoul National University, Seoul 06288, South Korea (e-mail: yoonchan@snu.ac.kr).

This article has supplementary downloadable material available at http://ieeexplore.ieee.org, provided by the authors.

Color versions of one or more of the figures in this article are available online at http://ieeexplore.ieee.org.

Digital Object Identifier 10.1109/JQE.2020.2968854

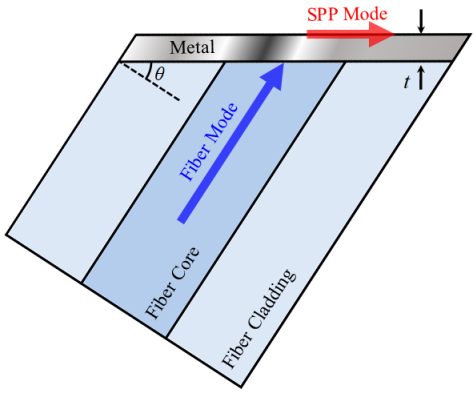

Fig. 1. Schematic of an MCAFF and its principle.

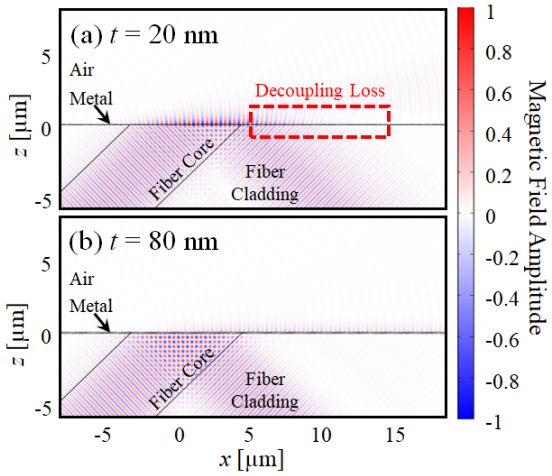

Fig. 2. Typical field patterns across two different MCAFFs when their metal thicknesses are set by (a) 20 nm and (b) 80 nm, respectively.

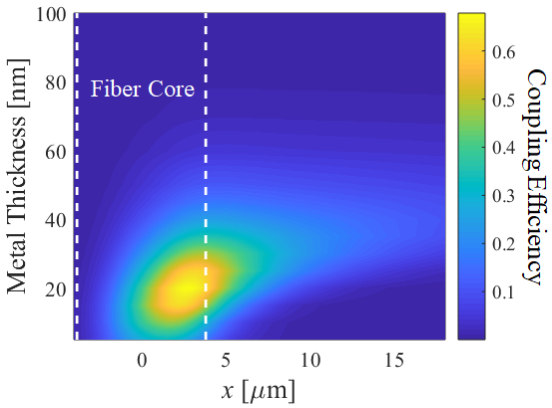

Fig. 3. SPP conversion efficiency for an MCAFF along the metal layer with respect to the thickness of the metal layer.

that SPPs are excited when the wavenumber of the incident fiber mode in the direction parallel to the metal-dielectric interface matches that of the desired SPP mode (see Fig. 1). The phase-matching condition for the wavenumber of the SPP mode is expressed as the following:

$$k_{SPP0} = n_{eff} k_0 \sin\theta, k_{SPP0} = k_0 \sqrt{\frac{\varepsilon_d \varepsilon_m}{\varepsilon_d + \varepsilon_m}} \quad (1)$$

where k_{SPP_0} is the wavenumber of the SPP mode,k_0 the wavenumber of the input radiation in free space, n_{eff} the effective refractive index of the optical fiber mode, θ the fiber facet angle, ε_d the electric permittivity of the dielectric (air in this case), and ε_m the electric permittivity of the metal.

A. Numerical Simulations

To justify how SPPs are generated under the MCAFF scheme, we have performed numerical simulations based on the finite element method (FEM: COMSOL Multiphysics®). We assumed the metal layer to be made of silver and the other simulation parameters to be as the following: the input radiation wavelength of 650 nm, the core diameter of the fiber of 5.3 μm, and the numerical aperture (NA) of the fiber of 0.14. This set of parameters leads to single-mode operation in the fiber for the input radiation of the given wavelength.

Typical SPP-field patterns are shown in Fig. 2 for a fiber tip angle θ of 46° with the metal layer thickness t of 20 and 80 nm, respectively. (We note that whilst the ideal phase-matching angle derived from Eq. (1) has been calculated to 44.56°, an MCAFF has quite broad angular bandwidth, which is typically given by a few degrees across the center angle [20].) From them, one can see that regardless of the thickness of the metal layer the incident optical fiber mode is initially coupled into an SPP mode at the metal-dielectric interface, which unidirectionally propagates to the right along the metal-dielectric interface. However, one can also notice that there are significantly different features in them in terms of what kind of SPP mode is dominantly excited and how it behaves while propagating along the metal-dielectric interface. In the case of a relatively thin metal layer, i.e., $t = 20$ nm, as shown in Fig. 2(a), SPP modes are strongly generated from the fiber core, but they are considerably localized in the region nearby the fiber core only. This indicates rapid decrease of the SPP modes by the decoupling loss, which is in fact incurred by the decoupling of the SPP modes back into optical fiber modes while propagating along the free metal-dielectric interface off the core region [16], [20]. On the other hand, in the case of a relative thick metal layer, i.e., $t = 80$ nm, as shown in Fig. 2(b), SPP modes are generated with relatively low intensity in comparison with that of the thin metal layer. However, they propagate with significantly low decoupling or leakage loss [1], [18].

Thus, we have calculated the SPP coupling efficiency with respect to the position x and the metal layer thickness t, which is shown in Fig. 3. We note that the SPP power was calculated by integrating the power flow based on the corresponding Poynting vector from the surface of the metal to the height of 1 μm above the metal-air interface normalized relative to the power flow of the fiber-optic input, which, in fact, results in the optic-to-SPP coupling efficiency. One can see that within or nearby the core region, the SPP coupling efficiency is clearly maximized if the metal thickness is as thin as $\sim$ 20 nm; however, the metal thickness for the maximal SPP strength

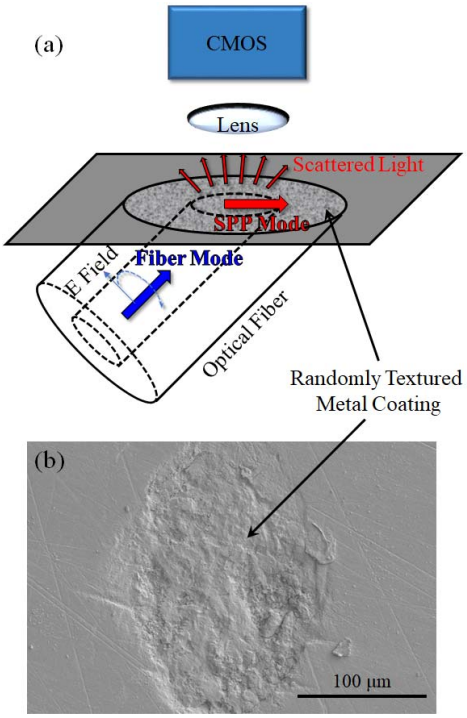

Fig. 4. Experimental demonstration of an MCAFF: (a) Experimental arrangement for characterization. (b) SEM image of its texturized surface.

tends to increase to $\sim$ 30 to 40 nm as the region of interest moves beyond the core region.

This is due to the fact that if the metal layer is as thin as $\sim$ 20 nm, SPP modes strongly coupled at the core region inevitably undergo considerably high decoupling loss. That is, it is very hard for them to reach the region relatively far off the region where they are initially excited, thereby tending to be localized within or nearby the core region. Thus, to make SPP modes reach the far-off region from the core with good efficiency, an appropriate metal thickness should be in the range of 30 to 40 nm.

B. Experimental Proof-of-Principle Test

To verify the functionality of the proposed MCAFF scheme, we have carried out a preliminary experiment as illustrated in Fig. 4(a) [16], [17]. The optical fiber was based on HI-1060, the core diameter and NA of which were given by 5.3 μm and 0.14, respectively. One fiber end was angle-cleaved to have the fact angle of $\theta = 46°$, which is near the exact phase-matching angle obtained by Eq. (1). The facet of the angled fiber end was polished with coarse sandpaper before the metal coating process in order for the fiber fact to be randomly texturized. At the end, silver was deposited onto the fiber facet by the electron-beam evaporating method. The thickness of the silver layer was set to $\sim$ 20 nm, where the outcoupling intensity was highest in our numerical simulations [See Fig. 3.].

We note that the metal-coated, randomly texturized surface facilitates the out-coupling of SPP modes into free-space modes as if it functioned as a random grating structure across the silica-metal interface [21]. A scanning electron microscope

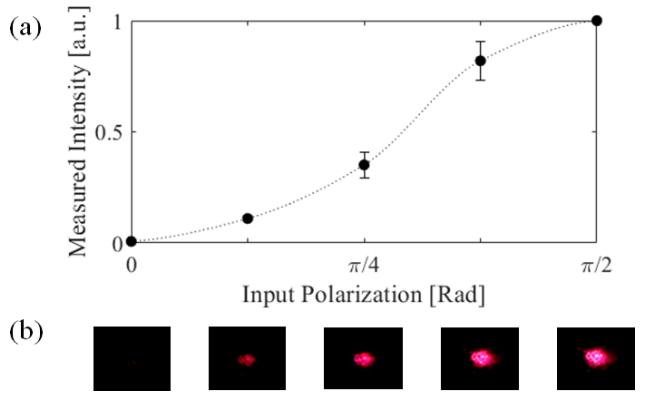

Fig. 5. Experimental result: (a) Out-coupled light of the texturized MCAFF with respect to incident polarization angle. (b) Corresponding CMOS image of the light transmission from the texturized MCAFF.

(SEM) image of the randomly texturized MCAFF is shown in Fig. 4(b). Next, to obtain the field intensity pattern of the coupled SPP modes in the MCAFF, light from a polarization-tunable source operating at 650 nm was launched into the other end of the fiber. In fact, the out-coupling of the SPP modes by the randomly texturized surface may appear only when TM modes are incident into the MCAFF. This is because SPP modes can only be generated by TM modes [1], [2].

The total power of the out-coupled (or transmitted) light through the randomly texturized MCAFF (RT-MCAFF) is illustrated with respect to incident polarization angle in Fig. 5 in an arbitrary unit normalized the maximum transmission, in which the corresponding images of the fiber facet observed with a CMOS camera are also presented. We note that 0 and $\pi/2$ of the incident polarization angle denote the TE and TM polarization states from the viewpoint of the RT-MCAFF, respectively. One can verify that out-coupled (or transmitted) light was maximized for the TM incident mode while it was nearly entirely diminished for the TE incident mode, as expected. We also provide a supplementary multimedia file for the detected CMOS image of the out-coupled light from the RT-MCAFF, from which one can see that the intensity of the out-coupled light varies with the polarization angle of incident light.

III. Two-Level-Thickness MCAFF

As mentioned in the preceding section, the SPP coupling efficiency within or nearby the core can increase with decreasing the metal layer thickness down to $\sim$ 20 nm; however, too thin a thickness can potentially cause a substantial level of propagation loss beyond the core region. Thus, one can think of a modified design for an MCAFF to compromise between the coupling efficiency and the propagation loss, in which the metal layer has a reduced thickness within the core region while it remains to have a sufficiently large thickness beyond the core region. Figure 6(a) depicts the schematic of a modified two-level-thickness MCAFF (TLT-MCAFF) designed for that purpose, in which the transitional regions (length: 2.2875 μm) between the thin and thick zones are adiabatically connected based on a cubic function

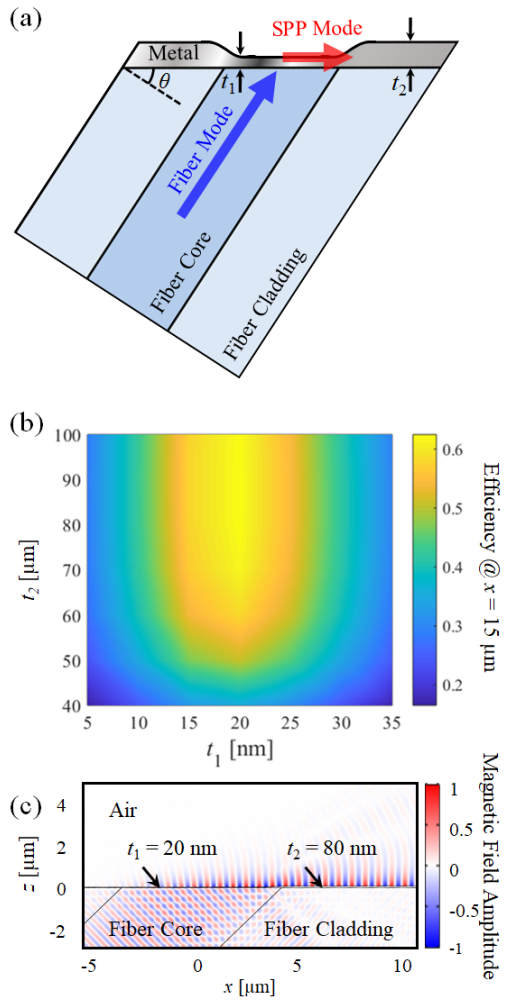

Fig. 6. Characteristics of a TLT-MCAFF: (a) Schematic of a TLT-MCAFF. (b) SPP coupling efficiency with respect to t_1 and t_2. (c) Field pattern.

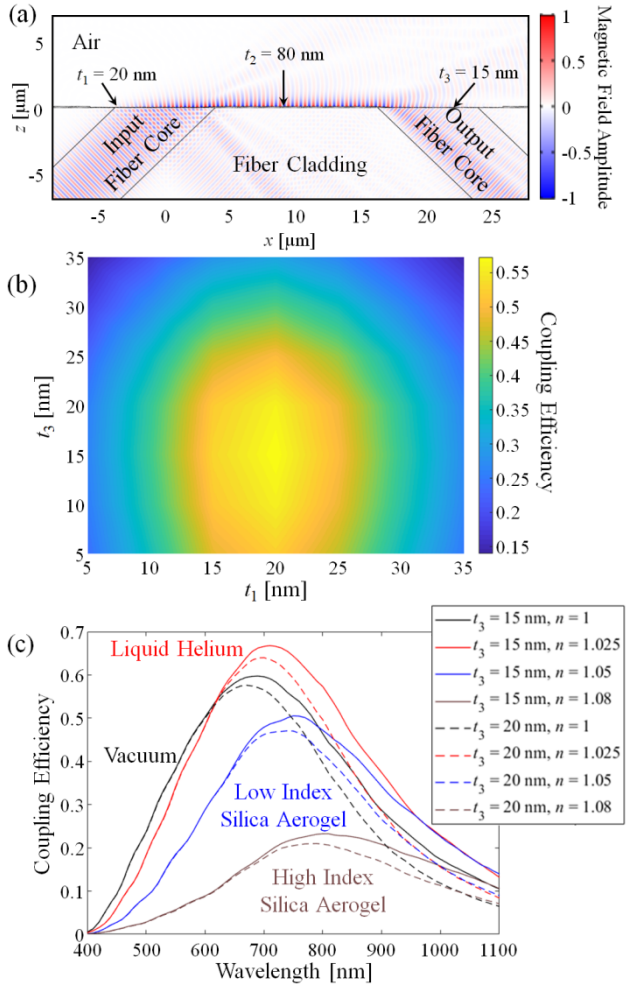

Fig. 7. FIFO-MCAFF platform for sensing applications: (a) Schematic and field pattern. (b) Coupling efficiency with respect to t_1 and t_2. (c) Coupling efficiency spectra for various different materials.

for simplicity. (We note that whilst we did not optimize the shape of the connecting formula, the given cubic function was good enough for avoiding undesirable back reflection effects.) Varying the two individual thicknesses of the metal sections, i.e., t_1 and t_2, we have calculated the SPP coupling efficiency at $x = 15$ μm, which is illustrated in Fig. 6(b). We note that all the other parameters remained identical to the preceding simulation shown in Fig. 3. From the result shown in Fig. 6(b), one can see that the thickness of t_2 of > 60 nm leads to significant enhancement in terms of the propagation loss in comparison with that shown in Fig. 3. The field pattern calculated for a typical case with $t_1 = 20$ nm and $t_2 = 80$ nm, is shown in Fig. 6(c), which eventually results in the SPP coupling efficiencies of 72.93 %, 62.39 %, and 53.49 % for $x = 5$, 15, and 25 μm, respectively. In comparison with the result shown in Fig. 2, one can see that the TLT-MCAFF not only produces high SPP coupling efficiency at the core region as shown in Fig. 2(a) for the thin uniform MCAFF, but also avoids unwanted decoupling loss as shown in Fig. 2(b) for the thick uniform MCAFF.

The TLT-MACFF can further be exploited into various fiber-based plasmonic devices [16]–[20]. In particular, the time-reciprocity elucidates that it can also receive SPP signals and convert them into optical fiber modes. This implies that it can be exploited into a FIFO plasmonic device if a pair of them are combined together. This serialized TLT-MCAFF pair can form an all-fiberized plasmonic transmitter-receiver, i.e., transceiver, which is fully compatible with fiber-optic systems, thereby having no alignment issues. We note that although SPP based research has been intensively carried out, there has been little effort paid to realization of plasmonic transceiver functionality [16], [19], [22]. Thus, we stress that the FIFO-plasmonic device can open up possibilities of being widely utilized as an align-free platform for SPP-based interconnection or sensing [23]. We here devise a schematic configuration of the FIFO-MCAFF transceiver as illustrated in Fig. 7, verifying its characteristics via numerical modeling and simulations. We note that the air region above the metal layer shown in Fig. 7 can be replaced with any gas, liquid, or even a biological sample, so that this device can function as a novel sensor platform that can fully exploit both the large bandwidth of optical fibers and the high resolution of SPP signals. For numerical characterization, we have assumed the thickness of the metal layer at the coupling zone (i.e., t_1),

and the thickness of the metal layer at the connecting or bridge zone (i.e., t_2), and the separation between two fiber centers to be 20 nm, 80 nm, and 20 μm, respectively. We also note that all the other parameters remained identical to those specified in the preceding simulation shown in Fig. 6. Figure 7(a) shows the device geometry and the corresponding field pattern for irradiation at 650 nm from the fiber placed on the left. In fact, the left fiber functions as a transmitter whereas the right fiber functions as a receiver. When the incident light from the core of the first fiber encounters the metal surface, it is coupled into an SPP mode. It then propagates along the metal surface over the bridge zone and is finally coupled back into to the second fiber on the right. Based on our numerical model, the calculated optical-to-optical coupling efficiency is as high as 57.62 % in the given parameter set.

To see how we can maximize its efficiency, we have then calculated the overall coupling efficiency, varying the thickness parameters for the transmitting MCAFF, the bridge, and the receiving MCAFF, i.e., t_1, t_2, and t_3 as shown in Fig. 7(a). The corresponding results are presented in Fig. 7(b). We note that the t_1 and t_3 parameters for the transmitting MCAFF and the receiving MCAFF do not have to be identical if we only consider using the platform for a unidirectional FIFO coupling purpose. In this case the MCAFF on the right is only required to function as a receiver, the functionality of which is actually maximized with 15 nm rather than with 20 nm in terms of t_3 when $t_1 = 20$ nm. Notwithstanding, we also note that if t_3 is set to be identical to t_1, the platform forms a symmetric geometry, so that one can use it for a bidirectional FIFO coupling purpose. In fact, we have numerically analyzed that the symmetric geometry with $t_1 = t_3 = 20$ nm yields the overall coupling efficiency of 56.00 %, which is only 1.62-%-point lower than the asymmetric case (57.62 % for $t_3 = 15$ nm). That is, it might be insignificant to set t_3 to be the same as t_1 if the symmetric geometry is preferred to allow for a bidirectional FIFO interconnection capability. To verify the characteristic efficacy of the FIFO-MCAFF platform from the viewpoint of plasmonic interconnection circuitry we further analyze its overall coupling efficiency, varying both wavelength of incident light and refractive index of the top layer of the FIFO-MCAFF platform, which is shown in Fig. 7(c). We have assumed that the refractive index of the top layer material can change by simply putting a new material on top of the FIFO-MCAFF platform. As typical examples, we choose four difference cases having refractive indices near unity, which are very hard to distinguish and identify with conventional techniques other than delicate interferometry techniques [24]: vacuum, liquid helium, and two types of silica aerogel, the refractive indices of which are given by 1, 1.025, 1.05, and 1.08, respectively. The solid and dashed lines denote the corresponding results for $t_3 = 15$ nm and $t_3 = 20$ nm, respectively. We highlight that the coupling spectrum is extraordinarily sensitive to detect a minute change in the refractive index of the object placed on top of the FIFO-MCAFF platform. Thus, once this platform is combined with a supercontinuum or tunable light source [25], it will provide an efficient way to gas or liquid sensing and detection.

IV. Conclusion

We have analyzed a novel metal-coated fiber-optic platform for SPP generation and interconnection that exploits an MCAFF configuration. The novel platform enables alignment-free unidirectional SPP generation with high efficiency and high flexibility. We have verified its effective functionality by means of rigorous numerical simulations as well as a preliminary experimental demonstration. In fact, the TLT-MCAFF configuration dramatically helps suppress the SPP decoupling loss, so that we have numerically verified that an optimized TLT-MCAFF parameterized with $t_1 = 20$ nm and $t_2 = 80$ nm can yield SPP coupling efficiency of up to 72.93% at the distance of 5 μm from the center of the core of the MCAFF. Exploiting the TLT-MCAFF configuration, we have also devised a FIFO platform for plasmonic interconnection and sensing, which consists of transmitting and receiving MCAFFs and a bridging channel. We have numerically verified that a FIFO platform parameterized with $t_1 = 20$ nm, $t_2 = 80$ nm, and $t_3 = 15$ μm can yield SPP coupling efficiency of up to 66.78 % at wavelength of 710 nm if its top layer is filled with liquid helium, for example. We have found that the peak SPP coupling efficiency as well as the peak wavelength are critically correlated with the refractive index of the top layer material, so that it can provide an efficient way to sensing volatile gas- or liquid-phase samples having refractive indices near unity with extraordinarily high sensitivity. We expect that the metal-coated fiber-optic platform based on the MCAFF configuration will be an efficient SPP generation and interconnection scheme enabling a lot of useful sensing and detection applications involving materials with refractive indices near unity, in particular.

References

[1] S. A. Maier, *Plasmonics: Fundamentals and Applications*. New York, NY, USA: Springer-Verlag, 2007.

[2] M. L. Brongersma, and P. G. Kik, *Surface Plasmon Nanophotonics*. New York, NY, USA: Springer-Verlag, 2007.

[3] H. Kim and Y. Jeong, "Theoretical and numerical study of cylindrical-vector-mode radiation characteristics in periodic metallic annular slits and their applications," *Curr. Opt. Photon.*, vol. 2, no. 5, pp. 482–487, 2018.

[4] H. Kim, "Metallic triangular pillar grating arrays for high transmission polarizers for air: Glass interfaces," *Jpn. J. Appl. Phys.*, vol. 58, no. 4, Apr. 2019, Art. no. 042001.

[5] K. J. Moh, X.-C. Yuan, J. Bu, S. W. Zhu, and B. Z. Gao, "Radial polarization induced surface plasmon virtual probe for two-photon fluorescence microscopy," *Opt. Lett.*, vol. 34, no. 7, p. 971, Apr. 2009.

[6] W. Chen, D. C. Abeysinghe, R. L. Nelson, and Q. Zhan, "Plasmonic lens made of multiple concentric metallic rings under radially polarized illumination," *Nano Lett.*, vol. 9, no. 12, pp. 4320–4325, Dec. 2009.

[7] S.-Y. Lee, "Design of a plasmonic switch using ultrathin Chalcogenide phase-change material," *Curr. Opt. Photon.*, vol. 1, no. 3, pp. 239–246, 2017.

[8] H. Kim and S.-Y. Lee, "Optical phase properties of small numbers of nanoslits and an application for higher-efficiency Fresnel zone plates," *Curr. Opt. Photon.*, vol. 3, no. 4, pp. 258–291, 2019.

[9] E. Kretschmann, "Die bestimmung optischer konstanten von metallen durch anregung von oberflächenplasmaschwingungen," *Z. Physik*, vol. 241, no. 4, pp. 313–324, Aug. 1971.

[10] B. Lee, Y.-B. Chen, and Z. Zhang, "Confinement of infrared radiation to nanometer scales through metallic slit arrays," *J. Quant. Spectrosc. Radiat. Transf.*, vol. 109, no. 4, pp. 608–619, Mar. 2008.

[11] C. Ropers, C. C. Neacsu, T. Elsaesser, M. Albrecht, M. B. Raschke, and C. Lienau, "Grating-coupling of surface plasmons onto metallic tips: A nanoconfined light source," *Nano Lett.*, vol. 7, no. 9, pp. 2784–2788, Sep. 2007.

[12] C. Guan *et al.*, "Compact all-fiber plasmonic Airy-like beam generator," *Opt. Lett.*, vol. 39, no. 5, p. 1113, Mar. 2014.
[13] G. Kostovski, P. R. Stoddart, and A. Mitchell, "The optical fiber tip: An inherently light-coupled microscopic platform for micro-and nanotechnologies," *Adv. Mater.*, vol. 26, no. 23, pp. 3798–3820, Jun. 2014.
[14] W. Chen, W. Han, D. C. Abeysinghe, R. L. Nelson, and Q. Zhan, "Generating cylindrical vector beams with subwavelength concentric metallic gratings fabricated on optical fibers," *J. Opt.*, vol. 13, no. 1, Jan. 2011, Art. no. 015003.
[15] H. Kim *et al.*, "Theoretical study on the generation of a low-noise plasmonic hotspot by means of a trench-assisted circular nano-slit," *Opt. Express*, vol. 22, no. 22, p. 26844, Nov. 2014.
[16] H. Kim, "Development of novel surface plasmon-based metal coated fiber-facets and their applications," Ph.D. dissertation, Seoul Nat. Univ., Seoul, South Korea, 2016.
[17] H. Kim, Y. Lee, H. An, L. A. Vazquez-Zuniga, B. Lee, and Y. Jeong, "Metal-coated angled fiber facet for surface plasmon generation," presented at the APLS, Jeju, South Korea, May 2016, Paper Thu-P-32.
[18] Y. Jeong and H. Kim, "Apparatus for excitation of surface plasmon wave," KR Patent 101 753 898, Jun. 28, 2017.
[19] H. Kim, H. An, J. Kim, and Y. Jeong, "All-fiberized surface plasmon transmitter-receiver," presented at the APC, Vancouver, BC, Canada, Jul. 2016, Paper SeW3E.5.
[20] H. Kim *et al.*, "Corrugation-assisted metal-coated angled fiber facet for wavelength-dependent off-axis directional beaming," *Opt. Express*, vol. 25, no. 7, p. 8366, Apr. 2017.
[21] I. I. Smolyaninov, D. L. Mazzoni, and C. C. Davis, "Imaging of surface plasmon scattering by lithographically created individual surface defects," *Phys. Rev. Lett.*, vol. 77, no. 18, pp. 3877–3880, Jul. 2002.
[22] W. Heni *et al.*, "High speed plasmonic modulator array enabling dense optical interconnect solutions," *Opt. Express*, vol. 23, no. 23, Nov. 2015, Art. no. 29746.
[23] E. Klantsataya, P. Jia, H. Ebendorff-Heidepriem, T. Monro, and A. François, "Plasmonic fiber optic refractometric sensors: From conventional architectures to recent design trends," *Sensors*, vol. 17, no. 12, p. 12, Dec. 2016.
[24] S. Lichtenberg, C. Heinisch, V. Petrov, J. Petter, and T. Tschudi, "Refractive-index measurement of gases with a phase-shift keyed interferometer," *Appl. Opt.*, vol. 44, no. 22, p. 4659, Aug. 2005.
[25] Y. Kwon, L. A. Vazquez-Zuniga, K. Park, S. Lee, H. Chang, and Y. Jeong, "Combinatorial study of supercontinuum generation dynamics in photonic crystal fibers pumped by ultrafast fiber lasers," *IEEE J. Quantum Electron.*, vol. 52, no. 6, pp. 1–11, Jun. 2016.

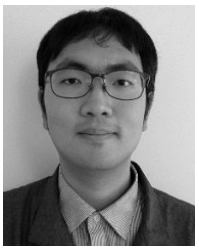

Hyuntai Kim received the Ph.D. degree from the School of Electrical Engineering, Seoul National University (SNU), South Korea, in 2016. He subsequently held a Postdoctoral Fellowship at SNU, for one year. He joined the Optoelectronics Research Centre (ORC), University of Southampton, as a Research Fellow, in 2017. Since 2019, he has been with the Department of Electronic and Electrical Converged Engineering, Hongik University, as a Faculty Member (Assistant Professor). He is primarily interested in fiber optics and nanophotonics.

Yoonchan Jeong (Member, IEEE) received the Ph.D. degree from the School of Electrical Engineering, Seoul National University (SNU), South Korea, in 1999. He subsequently held a Postdoctoral Fellowship at SNU, for two years. In 2001, he joined the Optoelectronics Research Centre, University of Southampton, as a Research Fellow, and became a Reader in 2006. He returned to the Department of Electrical and Computer Engineering, SNU, as a Faculty Member, in 2010. He has authored or coauthored over 300 publications, including patents, book contributions, and journal/conference papers. His early research covered holography, displays, fiber and waveguide optics, nonlinear optics, and lasers. His current research interests include high-power and ultrafast fiber lasers, laser physics, and quantum photonics. He has served on various committees for international photonics conferences and societies, including Fiber Lasers VI: Photonics West from 2008 to 2013 and Advanced Solid-State Lasers/Photonics from 2011 to 2016, and has been serving for Optical Sensors, leading the Laser Based Sensors subcommittee since 2015. He has served as an Associate Editor of the *Optics Express* from 2009 to 2016 and a Steering Committee Member for Siegman International School on Lasers from 2013 to 2016. He has been serving as the Editor-in-Chief for *Current Optics and Photonics* since 2019.